RSC Advances

ROYAL SOCIETY OF CHEMISTRY

www.rsc.org/advances

Co-delivery of doxorubicin and curcumin by polymeric micelles for improving antitumor efficacy on breast carcinoma

Lu Sun [1], Xiaohui Deng [2], Xi Yang [1], Zhaojun Li [1], Zhihan Wang [1], Ling Li [1], Qinjie Wu [1], Feng Peng [1], Lei Liu [1,*], Changyang Gong [1,*]

[1] Department of Medical Oncology, Cancer Center, State Key Laboratory of Biotherapy/Collaborative Innovation Center of Biotherapy, West China Hospital, Sichuan University, Chengdu, 610041, P. R. China

[2] Department of Human Anatomy, Xinxiang Medical University, Xinxiang, 453003, P. R. China

* To whom correspondence should be addressed (C Gong and L Liu). Tel: 86-28-85164063, Fax: 86-28-85164060, E-mail: chygong14@163.com and liuleihx@gmail.com.

Abstract

To date, combination chemotherapy has become a standard regimen to treat cancer patients. However, combination therapy with drugs having distinct properties such as solubility generally requires use of multiple carriers or solvents, which limits the likelihood of simultaneous delivery. In this work, we used biodegradable poly(ethylene glycol)-poly(ε-caprolactone) (mPEG-PCL) micelles as the co-delivery system to load hydrophilic doxorubicin (Dox) and hydrophobic curcumin (Cur) to achieve combination therapy. The co-encapsulation of Dox and Cur into mPEG-PCL micelles were prepared by a simple self-assembly procedure, which was absent of organic solvents, surfactants and vigorous stirring. The prepared Dox and Cur co-loaded micelles (Dox-Cur-M) were monodisperse with small particle size, high encapsulation efficiency (EE) and sustained release behavior. Furthermore, we found the Dox-Cur-M had remarkable progress in either cytotoxic activities or apoptotic effects compared with Dox-M or Cur-M at equivalent concentration, which was primarily attributed to enhanced cellular uptake of Dox by Cur. In addition, in subcutaneous 4T1 breast tumor model *in vivo*, the Dox-Cur-M was more effective in suppressing tumor growth and spontaneous pulmonary metastasis in comparison with the same dose of Dox-M and Cur-M. In conclusion, micellar co-delivery of Dox and Cur could synergistically potentiate antitumor effects on breast tumor.

Key words: combination therapy; micellar co-delivery; biodegradable; tumor

1. Introduction

Cancer remains a major public health problem around the world and one in four deaths in the United States are due to cancer. Breast cancer is the leading cause of cancer death among women aged 20 to 59 years, and is expected to account for 29% of all new cancer cases among women in 2014.[1] As a conventional treatment for breast cancer, chemotherapy continues to improve outcomes and still plays a critical role in management.[2, 3] However, chemotherapeutic drugs do not greatly discriminate between cancerous and normal cells, resulting in undesirable severe side effects. In addition, some anticancer drugs have limited water solubility and short blood circulation time in the body, leading to frequent administrations.[4] To combat these problems, a diverse assortment of delivery vehicles, such as polymer-drug conjugates, liposomes, micelles, nanogels, microspheres and nano-spheres, have been engineered to increase the drug concentration at the tumor site and/or decrease the exposure in normal host tissues, thus improving therapeutic efficacy and reducing toxicity and frequency of drug administration. [5-8]

In recent years, biodegradable polymeric micelles have attracted increasing attention due to the potential use as delivery vehicles for chemo-therapeutic drugs and the studies have demonstrated that these nanocarriers can significantly enhance the anti-tumor efficiency of various chemotherapeutic drugs.[9-13] Polymeric micelles are nanoscale core/shell structures usually formed through the self-assembly of amphiphilic block copolymers. The hydrophobic segments become packed together in aggregates (core), which serves as a storage site for poorly water-soluble drugs and

can act as a nano-depot for these agents. The hydrophilic shell commonly consisting of poly(ethylene glycol) (PEG) allows for increased water solubility, prolonged blood circulation, reduced protein adsorption and recognition by the mononuclear phagocytic system.[14-16] Besides, their nanosize gives rise to passive accumulation in tumor tissues based on the enhanced permeability and retention (EPR) effect.[17]

However, due to the heterogeneity of cancer cells, single agent therapy is restricted and combination chemotherapy has become a standard regimen to treat cancer patients. Drug combinations could produce a higher response rate or longer survival time than is possible with each drug used alone at its optimum dose. Furthermore, combinations of two or more agents can overcome toxicity and other side effects that limit the utility of many potential drugs, by either countering biological compensation, or accessing context-specific multi-target mechanisms.[18-20] But combination therapy with drugs having distinct properties such as solubility generally requires use of multiple carriers or solvents, limiting the likelihood of simultaneous delivery. Thus, there is a clear need to find a co-delivery system for loading different chemotherapeutic drugs with different physiochemical properties to achieve combination therapy after a single injection. The many multifunctional delivery systems have been designed for co-delivery of different guests, including micelles[21], liposomes[22] and inorganic nanoparticles[23], but co-delivery of chemotherapeutic drugs with distinct solubility characteristics is not easy to realize.

In this work, we successfully load water soluble Dox and insoluble Cur into biodegradable polymeric micelles to begin pursuing the goal of combination therapy.

Dox and Cur are drugs with different anticancer mechanisms[24-26], but recent studies have shown that regimens which combine Dox with Cur increase tumor regression rates relative to the individual drugs.[27, 28] Although previous research by Jinghua Duan et al, have demonstrated that co-encapsulated doxorubicin and curcumin in poly(butycyanoacrylate) nanoparticles (PBCA-NPs) could result in good results, there were still some properties to be further improved, such as small particle size, encapsulation efficiency, controlled drug release behavior, as well as better therapeutic efficacy. Furthermore, as far as we know, little work has been done to prepare micelles for co-delivery of drugs without toxic organic solvents. In this study, we prepared poly(ethylene glycol)-poly(ε-caprolactone) (mPEG-PCL) micelles incorporated with both Dox and Cur (Dox-Cur-M) through a self-assembly procedure without any surfactants or additives, which could ensure the safety of the formulation both in the formation process and further clinical use. After the Dox-Cur-M were obtained, the physicochemical characteristics were systematically investigated, which could provide some useful and essential information for *in vitro* cell experiments and *in vivo* studies. Subsequently, antitumor activities of Dox-Cur-M were evaluated on breast cancer both *in vitro* and *in vivo*.

2. Materials and methods

2.1. Materials, cell lines, and animals

Monomethyl poly(ethylene glycol) (mPEG, Mn=2000, Fluka, USA), ε-caprolactone (ε-CL, Alfa Aesar, USA), stannous octoate (Sn(Oct)2, Sigma, USA), methanol (HPLC grade, Fisher Scientific, UK), acetonitrile (HPLC grade, Fisher

Scientific, UK), dimethyl sulfoxide (DMSO, KeLong Chemicals, China), 3-(4,5-dimethylthiazol-2-yl)-2,5-diphenyl tetrazolium bromide (MTT, Sigma, USA), Hoechst33258 (Sigma, USA), curcumin (Sigma, USA) and doxorubicin hydrochloride (Sigma, USA) were used without further purification. All other chemicals used in this study were of the highest purity available. Ultrapure water was used for the preparation of all solutions.

L929 cells and 4T1 cells were obtained from the American Type Culture Collection (ATCC, Rockville, MD), which were cultured in Roswell Park Memorial Institute 1640 medium (RPMI 1640, Gibco, USA) or Dulbecco's modified Eagle's medium (DMEM, Sigma, USA) containing 10% fetal bovine serum (FBS, Gibco, USA) in an incubator supplied with 5% CO_2 at 37^{o}C, respectively.

Female BALB/c mice (6-8 weeks old) were from the Laboratory Animal Center of Sichuan University. The animals were kept in a specified pathogen free (SPF) room maintained at 20-22^{o}C and 50-60% relative humidity, with free access to standard laboratory chow and water. Animal experiments were approved by the institutional animal care and use committee of Committee of Sichuan University (Chengdu, China). All mice were administered humanistic treatment throughout the experimental period.

2.2. Preparation and characterization of Dox-Cur-M

Dox-Cur-M was prepared by two steps. The first step was to acquire Cur micelles by a one-step solid dispersion method.[12] Briefly, Cur and mPEG-PCL copolymer were co-dissolved in 5 mL of dehydrated alcohol under moderate stirring.

Then, the dehydrated alcohol was removed using a rotary evaporator at 60°C to form homogenous coevaporation, followed by dissolving in distilled water at 60°C to obtain micelles-encapsulated Cur. Second, Dox was incorporated into Cur-M through a pH-induced self-assembly method.[29] Briefly, 0.1 mL of PBS (10×, pH 7.4) was added into 0.7 mL of Cur-M solution (Cur concentration: 1.5 mg/mL; mPEG-PCL copolymer concentration: 60 mg/mL), followed by dropping 0.2 mL of Dox aqueous solution (5 mg/mL) into the above solution under mild stirring. One hour later, the Dox-Cur-M was prepared. The Dox-Cur-M was first centrifuged at 13000 rpm for 10 min to remove non-encapsulated Cur, and then was centrifuged at 20000 rpm for 5 min through a filter with molecular weight cutoff (MWCO) of 3 kDa to remove non-encapsulated Dox. The prepared Cur-M and Dox-M also went through the process of purification to remove corresponding free Cur or Dox before applied in all performed experiments.

Particle size distribution spectra of prepared Dox-Cur-M was examined by a laser diffraction particle size detector (Nano-ZS 90, Malvern Instruments, UK). The temperature was kept at 25°C during the detection process. All results were the mean of three sample runs, and all data were expressed as the mean ± standard deviation (SD).

The morphology of Dox-Cur-M was observed using transmission electron microscope (TEM, H-6009IV, Hitachi, Japan). Dox-Cur-M was diluted with distilled water and placed on a copper grid covered with nitrocellulose. Samples were negatively stained with phosphotungstic acid and dried at room temperature.

Quantitative assay of Cur and Dox entrapped in the micelles was carried out by high performance liquid chromatography (HPLC, Waters Alliance 2695) equipped with a Waters 2998 detector. A reversed phase C18 column (4.6 × 250 mm, 5 μm, Inertsil/WondaSil, Japan) was used for chromatographic separation. The column temperature was kept at 30°C. The mobile phase for detection of Cur was 60:40 v/v mixture of acetonitrile: 1% acetic acid. For quantitative assay of Dox, the mobile phase was changed to methanol/acetonitrile/1% acetic acid 40:10:50 (v/v). The flow rate was maintained at 1 mL/min with an injection volume of 20 μL. The detection wavelength for Cur and Dox was set at 420 nm and 252 nm, respectively. The elution time of Cur and Dox under chromatographic conditions described above was 6.951 and 10.965 minutes. Drug loading (DL) and encapsulation efficiency (EE) of Dox and Cur from Dox-Cur-M were calculated according to equations (1) and (2).

$$DL=\frac{\text{Drug}}{\text{Polymer}+\text{Drug}}\times 100\% \quad (1)$$

$$EE=\frac{\text{Experimental drug loading}}{\text{Theoretical drug loding}}\times 100\% \quad (2)$$

Dox-Cur-M was kept at 4°C or 25°C after preparation, and the stability of Dox-Cur-M was evaluated qualitatively by the observation of aggregates. A homogeneously transparent solution implied stable of the Dox-Cur-M, whereas the presence of precipitation indicated instable.

2.3. *In vitro* release study

To determine the release kinetics of Cur from Cur-M or Dox-Cur-M and Dox from Dox-M or Dox-Cur-M *in vitro*, a volume of 1 mL of these solutions were placed

in dialysis bags with a 3.5 kDa molecular weight cutoff (MD 36 mm, Union Carbide Corporation, USA) and immersed into 10 mL of PBS (pH 7.4) containing Tween80 (0.5% wt) or PBS solution containing 10% FBS (pre-warmed to 37^{o}C). The experiments were conducted in an incubator shaker (HZ-8812S, Scientific and Educational Equipment Plant, Taicang, China) at 37^{o}C with horizontally gentle shaking (90 rpm).. At predetermined time point, all the release media were removed and replaced with pre-warmed fresh release media. In addition, 1 mL of the sample was collected from the removed incubation medium and stored at -20^{o}C until analysis. The drug concentration in the different samples was determined by HPLC as described previously. All the results were the mean of five sample runs, and all data were expressed as the mean ± SD.

2.4. Evaluation of cytotoxicity

In vitro cytotoxicity assays of Cur-M, Dox-M and Cur-Dox-M on 4T1 cells were performed by the MTT method. Briefly, 4T1 cells at a density of 3×10^3 cells/well were seeded into 96-well plates and grown in 100 μL of RPMI1640 medium for 24h. The cells were then exposed to a series of different concentrations of Cur-M, Dox-M or Dox-Cur-M for 48h. The concentration of Dox or Cur in Dox-Cur-M was the same as in Dox-M or Cur-M. The viability of cells, determined by the MTT assay, was expressed as a percentage of the absorbance measured in control cells. The results were represented as mean ± SD of six independent experiments. In addition, the cytotoxicity of mPEG-PCL copolymer on 4T1 cells and L929 cells was evaluated using MTT method presented above.

2.5. Apoptosis assay

Apoptosis was identified morphologically by Hoechst33258 staining. 4T1 cells were seeded onto acid etched glass coverslips at a density of 5×10^4 cells per well and incubated in 1 mL of growth medium overnight. The next day, cells were subjected to fresh medium containing desired concentrations of sterile normal saline (NS) as control, blank micelles, Cur-M, Dox-M and Dox-Cur-M for 48h. Samples were then fixed with 70% cold alcohol, washed again with PBS, stained with Hoechst33258, then mounted onto glass slides and the slides were examined using a fluorescent microscope (DM2500, LEICA, Germany). Five equal-sized fields were randomly examined in each treatment. The percentages of positive apoptotic cells in each 200× high-power field were denoted as the apoptotic index (AI) (%).

2.6. Cellular uptake study

Cellular uptake of different formulations of Dox in 4T1 cells were measured by flow cytometry. Briefly, 4T1 cells at log phase were seeded in 6-well plates with 2×10^5 cells per well and cultured in 1 mL of growth medium at 37^{o}C for 24h. The growth media were then discarded, and cells were incubated for 2h or 4h with serum-free medium embodying blank micelles, free Dox, Dox-M, free (Dox + Cur), Dox-M + free Cur and Dox-Cur-M at a final doxorubicin concentration of 500 ng/mL, respectively. The concentration of Cur either in free Cur or in Dox-Cur-M was 500 ng/mL. At definite time intervals, the media were removed and cautiously washed with PBS. For quantitation of intracellular Dox using FCM (FACSCalibur, BD, USA), at least 10000 cells were harvested from each sample. The Dox-derived

fluorescence from individual cells was detected, while excitation was with the 488 nm line of an argon laser and emission fluorescence between 564 and 606 nm was measured. To visualize Dox uptake of Dox-M and Dox-Cur-M by fluorescence microscopy, 4T1 cells at log phase were cultured in 6-well plates containing an acid etched glass coverslips with 2×10^5 cells per well for 24h. Then blank micelles, Dox-M and Dox-Cur-M were added to designated wells. After incubation for 2h and 4h, the media were removed and carefully washed with PBS. Cells were fixed with 70% cold alcohol, washed again with PBS, stained with Hoechst33258, and imaged using a fluorescence microscope. The Dox was excited with 543 nm laser and the emission wavelength was set from 580 to 620 nm. The nuclear dye was excited with 633 nm laser and observed at wavelength from 680 nm to 720nm and expressed as blue. Each condition was conducted in triplicate.

2.7. *In vivo* anti-tumor studies

In subcutaneous 4T1 breast tumor model, female BALB/c mice (6–8 weeks old) were subcutaneously inoculated with 5×10^5 of 4T1 cells suspended in 0.1 mL of serum free medium in the right flank on day 0. Tumors were allowed to grow for 4 days to achieve palpable before treatment, followed by tumor bearing mice randomly assigned to five groups (5 mice per group). On day 4, 7, and 10, mice were intravenously administrated with sterile NS (control), blank micelles, Cur-M (1 mg/Kg), Dox-M (1 mg/Kg) and Cur-Dox-M (dose of curcumin and doxorubicin both were 1 mg/Kg), respectively. Tumor size was measured every three days using calipers. Tumor volume was evaluated using the formula $vol = (a \times b^2)/2$, where vol is

tumor volume, a is the length of the major axis, and b is the length of the minor axis. On day 30, mice in control group began to die, and other mice were killed by cervical vertebra dislocation. Subsequently, their tumors were immediately harvested, weighed and analyzed. 4T1 breast tumor in BALB/c mice is with high propensity for hematogenously spread metastases, often leading to tumor burden in lungs.[30] Therefore, lungs in each group were promptly harvested and weighted, and number of tumor nodules was numbered in each lung by two investigators in a blinded fashion.

2.8. Quantitative examination of apoptosis

Tumor specimens in subcutaneous 4T1 model were collected, fixed in 4%wt paraformaldehyde (PFA), embedded in paraffin, and sectioned. Terminal deoxynucleotidyl transferase-mediated nick-end labeling (TUNEL) staining was perform using an in situ cell death detection kit (DeadEnd™ Fluorometric TUNEL System, Promega, Madison, USA) as illustrated by the manufacturer's protocol. The assay relies on the presence of nicks in the DNA which can be identified by terminal deoxynucleotidyl transferase, an enzyme that will catalyze the addition of dUTPs. Five equal-sized fields were randomly examined in tumor tissue sections. The percentages of TUNEL-positive apoptotic cells in each 200× high-power field were denoted as the apoptotic index (AI) (%).

2.9. Assessment of tumor proliferation

To quantify Ki-67 protein expression, tumor tissues were embedded in paraffin and cut to 5-μm-thick sections for Ki-67 staining using the labeled streptavidin-biotin method. The primary antibody was rat anti-mouse monoclonal antibody Ki-67 (Gene

Tech) and the secondary antibody was biotinylated goat anti-rat immunoglobulin (BD Biosciences Pharmingen). Positively staining cells from five tumors per group were counted in five randomly selected fields under 200× high-power magnification by two independent investigators in a blind. The Ki-67 labelling index (Ki-67 LI) was calculated as number of Ki-67-positive cells/total cell count × 100%.

2.10. Tumor microvessel density

Microvessel density (MVD) was viewed as a marker for tumor angiogenesis. Immunofluoresce detection of neovascularization in tumor tissue was performed to evaluate antiangiogenesis effect of Dox-Cur-M. Frozen sections of tumors were fixed in acetone, incubated, stained with an antibody reactive to CD31 (BD Pharmingen TM, USA), washed with PBS, and followed by incubation with a FITC-conjugated second antibody (Abcam, USA). MVD was determined by counting the number of microvessels per 200×high-power field in the sections under a fluorescence microscopy.

2.11. Statistical analysis

The statistical analysis was performed using SPSS version 17.0 (Chicago, IL, USA). Statistical comparisons were made with one-factor analysis of variance (ANOVA) with Dunnett-t test used for post hoc comparisons. Differences were considered statistically significant at $P < 0.05$ with a 2-tailed test.

3. Results

3.1. Preparation and characterization of Dox-Cur-M

We incorporated Cur and Dox into mPEG-PCL micelles by a simple self-assembly procedure, as shown Figure 1A. The procedure of preparing the Dox-Cur-M was very simple, and no surfactants, organic solvents or vigorous stirring were applied in this procedure. When the in-feed mass ratio of Dox, Cur and mPEG-PCL copolymer was 1:1:38, the average particle size of prepared Dox-Cur-M was 25.3 ± 0.2 nm with polydispersity index (PDI) of 0.065 ± 0.011. The particle size distribution spectrum of Dox-Cur-M was presented in Figure 1B, implying that those micelles encapsulating Dox and Cur were monodisperse. Dox and Cur were efficiently loaded in mPEG-PCL micelles, EE of Dox and Cur reaching 96.77 ± 0.30% and 99.32 ± 0.47%, and DL 4.85 ± 0.01% and 4.97 ± 0.02%, respectively. The morphology of the Dox-Cur-M, determined by TEM, was shown in Figure 1C. The image revealed that Dox-Cur-M was dispersed as individual particles with a well-defined spherical core-shell structure homogeneously distributed around a size of 25 nm. Consequently, these structural characteristics of Dox-Cur-M observed by TEM were consistent with the results of particle size analysis. In addition, we also reported particle sizes and TEM picture of blank micelles, Dox-M and Cur-M in the Figure S1 and Figure S2. As shown in Figure 1D, the aqueous solution of blank micelles, Dox-M, Cur-M and Dox-Cur-M are transparent and homogeneous. In addition, the Dox-Cur-M formulations stored at 25°C could be stable for 20 days, while at 4°C for up to one month with no aggregates.

3.2. *In vitro* drug release behavior

The *in vitro* release profiles of Cur from Cur-M or Dox-Cur-M and Dox from Dox-M or Dox-Cur-M were studied using a dialysis method. It was indicated from Figure 2 that both Cur and Dox from Dox-Cur-M showed a sustained release either in PBS (pH 7.4) or in 10% FBS over an extended period. As shown in Figure 2A and 2C, release rate of Cur from Dox-Cur-M was lower than that from Cur-M either in PBS (pH 7.4) or in 10% FBS, which may be attributed to competition between Cur and Dox in diffusing out from the micelles. In the 7th day, approximately 36% (no serum) and 78% (with serum) of Cur was released into the outside media in Cur-M group, whereas only 17% (no serum) and 50% (with serum) of Cur was released from Dox-Cur-M. Dox is a glycoside composed of a hydrophobic glycone linked to a hydrophilic glucosamine moiety. Dox attached to PCL comprising the core region might interact with the hydrophobic and hydrophilic moieties of the polymeric micelles with its glycoside groups in hydrophilic regions and other part in hydrophobic regions.[31] Consequently, it was found from Figure 2B and 2D that an initial burst release of Dox occurred in all groups compared with Cur, followed by a sustained release behavior. The cumulative release rate of Dox from Dox-Cur-M in the absence of serum or in the presence of serum was 49.71 ± 3.33% or 50.62 ± 0.72%, which was lower than that from Dox-M (57.43 ± 3.36% or 70.43 ± 0.87%, respectively).

3.3. Cytotoxicity studies

MTT assay was employed to further determine whether the associated encapsulation of Dox and Cur into the mPEG-PCL copolymer could enhance

cytotoxicity on 4T1 cells compared with Cur-M and Dox-M. It was evident from Figure 3A that the concentration of Dox-Cur-M that caused 50% killing was much lower than that of Dox-M (mean = 0.34 versus 0.94 μg/mL). However, 4T1 cells exposed to Cur-M at final concentration of 2.5 μg/mL remained high viability. Half maximal inhibitory concentration (IC_{50}) of Cur micelles was 9.70 μg/mL. Accordingly, the results were confirmed that Dox-Cur-M could remarkably improve cytotoxic activity.

4T1 and L929 cells were used to evaluate the cytotoxicity of blank mPEG-PCL micelles by a standard MTT assay. As shown in Figure 3B, we found that the viability of 4T1 and L929 cells were rather high, even when incubated at a final micelle concentration of 1000 μg/mL. These results suggested that mPEG-PCL copolymer were biocompatible with low cytotoxicity and could serve as a safe carrier.

3.4. Apoptosis assay

Hoechst33258 staining of DNA was performed to address whether the combined encapsulation of Dox and Cur into the micelles could reinforce apoptosis on 4T1 cells. Under the observation of fluorescence microscope, apoptotic cells showed a strong blue fluorescence in comparison with normal cells owing to nuclear fragmentation and chromatin condensation. Figure 4 presented the images of cells treated with NS (control), blank micelles, Cur-M, Dox-M and Dox-Cur-M for 48h. It was found that cells in Dox-Cur-M group experienced a more distinguished increase in apoptosis than those in Dox-M group. However, cells treated with blank micelles or Cur-M showed homogenous fluorescence with few evidence of segmentation and

fragmentation of nuclei. Similarly, as shown in Figure 4F, the apoptosis index in Dox-Cur-M group (38.30 ± 2.26%) was much greater than that in Dox-M (14.13 ± 0.28%, P<0.001, ANOVA), Cur-M (3.86 ± 0.34%, P<0.001, ANOVA), blank micelles (1.86 ± 0.10, P < 0.001, ANOVA), or NS group (2.14 ± 0.17%, P<0.001, ANOVA). Moreover, there was no statistical difference in the apoptosis index among NS, blank micelles and Cur-M group (P>0.05, ANOVA).

3.5. Cellular uptake studies

Dox-Cur-M illustrated a more powerful cytotoxic activity and apoptosis effect on 4T1 cells than Dox-M. However, the highest Cur concentration of Dox-Cur-M was far lower than IC_{50} of Cur. This makes us speculate that whether the Cur of Dox-Cur-M facilitated Dox to entry into cells. Hence, we studied internalization of Dox by fluorescent microscopy and flow cytometry. Figure 5 depicted the intracellular uptake of different formulations of Dox in 4T1 cells determined by FCM. It was found from Figure 5A, C, E that Dox in free Dox group was scarcely internalized by 4T1cells, while Dox in another four treatments continued to accumulate in varying degrees after 2h of incubation. Moreover, either the percentage of Dox-containing cells or mean fluorescence intensity in the Dox-Cur-M group (62.63 ± 5.17% and 51.57 ± 0.90) was much higher than those in the Dox-M + Free Cur (49.44 ± 8.40% and 48.73 ± 0.90, P<0.05, ANOVA), Dox-M (17.32 ± 3.44% and 44.66 ± 0.77, P<0.001, ANOVA)，free (Dox + Cur) (3.46 ± 0.47% and 41.73 ± 0.31, P<0.001, ANOVA) and free Dox group (0.21 ± 0.06% and 41.26 ± 0.19, P<0.001, ANOVA). As illustrated by Figure 5B, D, F, the internalized Dox of each treatment increased gradually at 4h. Similarly,

the maximum amount of Dox was accumulated in the cells treated with Dox-Cur-M group compared to free Dox, free (Dox + Cur) and Dox-M group, as evidenced by statistically significant difference in either the percentage of Dox-containing cells or mean fluorescence intensity ($P<0.001$, ANOVA). Simultaneously, more uptake of Dox was observed in Dox-Cur-M group in contrast to Dox-M + Free Cur group in 4h, but not a statistically significant difference between the two groups ($P>0.05$, ANOVA). Figure 6 exhibited the photographs of cells treated with blank micelles, Dox-M and Dox-Cur-M at 2h and 4h under a fluorescent microscopy, respectively. Taking advantage of nuclear staining using Hoechst33258, it was found that red fluorescence from Dox was localized in the nuclei. Images of cells incubated with empty micelles did not show any Dox-derived fluorescence at any time intervals. In Dox-M group, a quite weak Dox-derived fluorescence was viewed after 2h of incubation, while red fluorescence of Dox-Cur-M group was noticeably boosted. Dox continuing to rapidly accumulate in the nuclei during the 4h incubation, both of Dox-derived fluorescence in Dox-M and Dox-Cur-M group was enhanced. But a more bright red fluorescence was observed in the Dox-Cur-M group.

3.6. *In vivo* anti-tumor activity

We compare the antitumor effect of Dox-Cur-M with that of Dox-M, Cur-M, blank micelles, and NS in subcutaneous 4T1 breast carcinoma mouse model. As shown in Figure 7A and Figure 7B, Dox-Cur-M displayed a more drastic suppressive effect on tumor growth than Dox-M and Cur-M ($P<0.05$ and $P<0.001$, ANOVA), whereas blank micelles did not perform any antitumor effect compared with NS

(P>0.05, ANOVA). Figure 7C showed the weight of tumors in each group, and tumor weight in Dox-Cur-M group (0.51 ± 0.22 g) was far lower than that in Dox-M (1.27 ± 0.67 g, P<0.05, ANOVA), Cur-M (2.67 ± 1.10 g, P<0.001, ANOVA), blank micelles (4.39 ± 0.93 g, P<0.001, ANOVA), or NS group (4.09 ± 0.80 g, P<0.001, ANOVA). Furthermore, we explored inhibitory effect of Dox-Cur-M on spontaneous pulmonary metastasis of 4T1 breast carcinoma. As illuminated in Figure 8A and Figure 8B, there was a marked decline in mean number of tumor nodules of Dox-Cur-M group (6.0 ± 3.2) compared with that of Dox-M (15.20 ± 4.5, P<0.05, ANOVA), Cur-M (26.4 ± 6.2, P<0.001, ANOVA), blank micelles (49.4 ± 20.8, P<0.001, ANOVA), or NS group (46.2 ± 12.8, P<0.001, ANOVA). Figure 8C showed that weight of lung in Dox-Cur-M group is the lightest among the five groups. These findings implied Dox-Cur-M exerted a distinctly important role on suppression of tumor growth and metastasis.

3.7. Quantitative assessment of apoptosis

Immunofluorescent TUNEL staining assays was used to examine the effect of Dox-Cur-M on apoptosis in 4T1 tumors. Figure 9 showed representative images of apoptosis in 4T1 tumor sections of all five groups. The nuclei stained with green were an indication of apoptotic cells. It should be noted that more apoptotic cells in Dox-Cur-M group were observed compared with those in Dox-M, Cur-M, blank micelles, or NS group within an equal-sized high-power field. Figure 9F was clear reflection of the level of apoptosis index among five groups. The apoptosis index in Dox-Cur-M group (21.86 ± 2.42%) was much greater than in Dox–M (11.06 ± 2.05%,

P<0.001, ANOVA), Cur-M (5.86 ± 1.28%, P<0.001, ANOVA), blank micelles (3.18 ± 0.97%, P<0.001, ANOVA), or NS group (2.38 ± 0.99%, P<0.001, ANOVA).

3.8. Determination of tumor cell proliferation

We checked the hypothesis whether Dox-Cur-M was highly effective against the proliferation of tumor cells determined by immunohistochemical staining of Ki-67. In Figure 10, Ki-67 immunoreactivity of the tumors in Dox-Cur-M appeared to be weakest among five groups within an equal-sized high-power field. According to Figure 10F, Ki-67 LI in Dox-Cur-M group is 18.6 ± 6.5%, versus 40.4 ± 6.7% in Dox-M group (P<0.001, ANOVA), 58.6 ± 9.8% in Cur-M group (P<0.001, ANOVA), 70.4 ± 11.3% in blank micelles group (P<0.001, ANOVA), and 76.2 ± 8.0% in NS group (P<0.001, ANOVA). The results showed that Dox-Cur-M acted a pronounced role in anti-cell proliferation effect.

3.9. Inhibition of tumor angiogenesis

It has been well documented that tumor growth and metastases require new vasculature. To determine whether the reduced growth of tumors undergoing Dox-Cur-M treatment was associated with an antiangiogenic effect, we examined microvessel density (MVD) in tumor tissues by immunofluorescence CD31 staining assays. As shown in Figure 11, fewer immunoreactive microvessels (red fluorescence) in tumor tissues were observed in Dox-Cur-M group compared with those in Dox-M, Cur-M, blank micelles, or NS group. The Dox-Cur-M group was highly effective in suppressing angiogenesis as indicated by a lower MVD of 17.4 ± 6.1 than that of Dox-M group (54.2 ± 8.5, P<0.001, ANOVA), Cur-M group (43.2 ± 4.9, P<0.001,

ANOVA), blank micelles (62.2 ± 6.8, P<0.001, ANOVA), or NS group (63.6 ± 7.6, P<0.001, ANOVA) (as shown in Figure 11F).

4. Discussion

Combination of two or more agents, common approach in oncology, is a prospective strategy to improve therapeutic efficacy, overcome undesirable toxicity, reduce the dosage of each agent and achieve multiple targets. A step forward can be taken by loading different drugs onto a single carrier, allowing simultaneous delivery of both drugs. A reasonable election of the co-delivered drugs can improve the therapeutic index of the native drugs , leading to an overall enhanced anticancer activity.[32] It has been reported that methoxy poly (ethylene glycol)-poly (lactide-co-glycolide) (mPEG-PLGA) for co-delivery of Dox and paclitaxel (TAX) suppressed tumor cells growth more efficiently than the delivery of either Dox or TAX at the same concentrations, indicating a synergistic effect.[33] Also, co-delivery of a low molecular weight heparin (LMWH) taurocholate conjugate (LHT7) with suberoylanilide hydroxamic acid (SAHA), a histone deacetylase inhibitor, in nanolipoplex could provide synergistic antitumor effect.[34] In addition, ligand targeted-liposomal formulation of the anti-angiogenic agent Combretastatin A-4 (CA-4) and Dox was demonstrated to significantly prolong the concentration of the two drugs at the tumor site.[35] In this work, we anticipated that MPEG-PCL micelles for co-delivery of Dox and Cur could achieve synergistic effect, thus cytotoxicity in principle be maximized.

Recently, several examples of co-delivery systems for Dox and Cur have been

reported. Ranjita Misra *et al*. developed the co-delivery of Dox and Cur in poly (D,L-lactide-co-glycolide) (PLGA) NPs for enhancement of efficacy of Dox in K562 cells. However, anti-tumor effect of dual drug loaded NPs was only examined by some *in vitro* experiments, while *in vivo* assay was not involved in this research.[36] Dipankar Pramanik et al. synthesized a doxorubicin-curcumin composite nanoparticle formulation called NanoDoxCurc (NDC) for anti-cancer therapy.[37] But during the preparation process, chloroform was used to dissolve curcumin. Different from Dipankar Pramanik' study, we developed a novel micellar delivery system for effective co-delivery of the dual drugs by a simple self-assembly procedure without any toxic organic solvent, surfactant, or cryoprotector. Moreover, 4T1 breast tumor developed in BALB/c mice is highly metastatic and are able to spread into lungs, therefore, in the *in vivo* experiments, 4T1 breast tumor model was used to evaluate both anti-tumor and anti-metastasis activity of Dox-Cur-M in our study. Besides, we also examined whether the enhanced anti-tumor effect was attributed to curcumin-enhanced cellular uptake of doxorubicin of Dox-Cur-M.

One advantage of micelles with intrinsic core-shell architecture as drug delivery systems is the controlled drug release, which improves the drug bioavailability by the EPR effects.[17, 38] The *in vitro* release profiles of Cur-M, Dox-M, and Dox-Cur-M had been obtained either in PBS (pH 7.4) or in 10% FBS at 37°C, as is relevant to *in vivo* circulation. Both Dox and Cur was released from the polymeric vesicles in a controlled and sustained fashion. But Cur or Dox from Dox-Cur-M underwent a relatively lower cumulative release rate over an extended period in comparison with

Cur from Cur-M or Dox from Dox-Cur-M either in the presence of serum or in the absence of serum. Such slow release profile appeared to be a favorable feature for Dox-Cur-M, as the loaded drugs from Dox-Cur-M would be less likely leaching during the *in vivo* circulation before reaching the tumor, thus the effective release in tumor tissues for the desirable chemotherapy performance.

Dox can bind to DNA by intercalation and induces a series of biochemical events leading to apoptosis in a number of different tumor cells.[39] The curcumin, an orange-yellow polyphenol present in curry spice, has a long history of use for traditional therapies. Curcumin has been described as a potent antioxidant, anti-inflammatory agent and chemo-sensitizer in cancer chemotherapy.[25] Therefore, it is expected that curcumin can improve chemotherapy results of Dox. Several investigations were made in the present study concerning the antitumor activity of the Dox-Cur-M on breast carcinoma. *In vitro* assays, Dox-Cur-M was vastly superior to Dox-M either in cytotoxic activity or in apoptosis-inducing effect, and the highest concentration of Cur from Dox-Cur-M was further lower than the IC_{50} value. This is similar to what was observed in 4T1 breast tumor subcutaneous model *in vivo*, where the co-encapsulation of Cur and Dox into mPEG-PCL copolymer had huge advantages over Dox-M and Cur-M at equivalent dose in the inhibition of tumor growth and metastasis. Interestingly, immunofluorescent and immunohistochemical assays also convincingly showed that Dox-Cur-M made better in antitumor activities compared with Dox-M or Cur-M.

We examined the effects of Cur from Dox-Cur-M on cellular uptake of Dox, performed by fluorescence microscope and FCM, to clarify the mechanism responsible for higher cytotoxicity and enhanced apoptosis of Dox-Cur-M. For quantitation analysis of intracellular doxorubicin using FCM, both the percentage of Dox-containing cells and mean fluorescence intensity in Dox-Cur-M group were much higher than those in free Dox, Dox-M, free (Dox + Cur), Dox-M + free Cur group at 2h and 4h. Although the Dox-Cur-M promoted more internalization of Dox compared with Dox-M + free Cur, the uptake of Dox between the two treatment was not statistically significant different after 4h of incubation. Based on these results，it was inferred that at the initial stage Cur from dual drug loaded micelles led to higher DOX accumulation in the cells than free Cur, while the encapsulated Cur in dual drug loaded micelles did not further increased intracellular accumulation of Dox compared with free Cur after 4h of incubation. Consequently, the Cur in either case was the main reason responsible for the enhanced uptake of Dox. But our results were quite different from Y. Sadzuka's findings. They discovered that curcumin did not have any effect on Dox transport across the tumor cell membrane, after co-administration of Dox and Cur as a free drug cocktail.[40] However, how the Cur promoted the uptake of doxorubicin is worth further exploration. This phenomenon was also confirmed by visualizing doxorubicin uptake by fluorescence microscopy, the uptake of Dox in tumor cells was increased in a time-dependent manner in both the Dox-M group and the Dox-Cur-M group, but the internalization of Dox from Dox-Cur-M developed more rapidly than that from Dox-M. In addition, the cellular uptake of micelles most

likely occurs via endocytosis or potentially pinocytosis, in which lysosomes processing spark off a burst release of drugs into the cytosols. Since Dox is a DNA intercalating drug, it first has to diffuse out into the nucleus, and then could immediately exert its biological actions. In this study, we found that Dox from Dox-M or Dox-Cur-M had undergone nuclear internalization at 2h or even faster after the definite treatment. This phenomenon indicated that the triggering mechanism for the release of the Dox from the hydrophobic core region of micelles into the nucleus was highly efficient.

Taken together, the vigorous anticancer effect of Dox-Cur-M, compared with Cur-M and Dox-M, may result from the improved cytotoxicity, the enhanced apoptosis and the delayed release profile of Dox-Cur-M. Moreover, the study demonstrated that not only could Dox from Dox-Cur-M rapidly undergo nuclear internalization, but the Cur from Dox-Cur-M facilitated the cellular uptake of Dox.

5. Conclusions

In this work, we have successfully prepared mPEG-PCL micelles as carriers to co-deliver Dox and Cur for the controlled release in tumor therapy. The particle size and TEM image of the prepared Dox-Cur-M indicated its stability and solubility. The releases of Dox and Cur from Dox-Cur-M at 37°C and neutral pH were slow and sustained. Furthermore, the co-delivery nanocarrier exerted stronger antitumor activity on breast tumor either *in vitro* or *in vivo* than the delivery of either Dox or Cur at the same concentrations. In addition, we also suggested a possible mechanism

that the positive effects of Cur on the internalization of Dox *in vitro* were responsible for the enhancement of Dox-induced antitumor activity.

Acknowledgment

This work was financially supported by National Natural Science Foundation of China (NSFC81201724), Distinguished young scholars of Sichuan University (2013SCU04A16), Specialized Research Fund for the Doctoral Program of Higher Education (20120181120044).

Declaration of Interest statement

The authors report no conflicts of interest. The authors alone are responsible for the content and writing of the paper.

References

1. R. Siegel, J. Ma, Z. Zou and A. Jemal, *CA Cancer J. Clin.*, 2014, **64**, 9.
2. H. A. Azim, Jr., E. de Azambuja, M. Colozza, J. Bines and M. J. Piccart, *Ann. Oncol.*, 2011, **22**, 1939.
3. S. M. Swain, *Oncologist*, 2011, **16 Suppl 1**, 30.
4. T. M. Allen and P. R. Cullis, *Science*, 2004, **303**, 1818.
5. J. Shi, A. R. Votruba, O. C. Farokhzad and R. Langer, *Nano Lett.*, 2010, **10**, 3223.
6. H. Tang, C. J. Murphy, B. Zhang, Y. Shen, E. A. Van Kirk, W. J. Murdoch and M. Radosz, *Biomaterials*, 2010, **31**, 7139.
7. R. Patil, J. Portilla-Arias, H. Ding, B. Konda, A. Rekechenetskiy, S. Inoue, K. L. Black, E. Holler and J. Y. Ljubimova, *Int. J. Mol. Sci.* , 2012, **13**, 11681.
8. V. Lorusso, L. Manzione and N. Silvestris, *Ann. Oncol.*, 2007, **18 Suppl 6**, vi70.
9. L. Liu, L. Sun, Q. Wu, W. Guo, L. Li, Y. Chen, Y. Li, C. Gong, Z. Qian and Y. Wei, *Int. J. Pharm.*, 2013, **443**, 175.
10. C. Gong, S. Deng, Q. Wu, M. Xiang, X. Wei, L. Li, X. Gao, B. Wang, L. Sun, Y. Chen, Y. Li, L. Liu, Z. Qian and Y. Wei, *Biomaterials*, 2013, **34**, 1413.
11. Q. Wu, S. Deng, L. Li, L. Sun, X. Yang, X. Liu, L. Liu, Z. Qian, Y. Wei and C. Gong, *Nanoscale*, 2013, **5**, 12480.
12. C. Gong, Y. Xie, Q. Wu, Y. Wang, S. Deng, D. Xiong, L. Liu, M. Xiang, Z. Qian and Y. Wei, *Nanoscale*, 2012, **4**, 6004.
13. N. Tang, G. Du, N. Wang, C. Liu, H. Hang and W. Liang, *J. Natl. Cancer Inst.*, 2007, **99**, 1004.
14. H. M. Aliabadi, M. Shahin, D. R. Brocks and A. Lavasanifar, *Clin. Pharmacokinet.*, 2008, **47**,

619.
15. W. H. De Jong and P. J. Borm, *Int. J. Nanomedicine*, 2008, **3**, 133.
16. S. R. Croy and G. S. Kwon, *Curr. Pharm. Des.*, 2006, **12**, 4669.
17. H. Maeda, *Bioconjug. Chem.*, 2010, **21**, 797.
18. W. G. Kaelin, Jr., *Nat. Rev. Cancer*, 2005, **5**, 689.
19. C. J. Torrance, P. E. Jackson, E. Montgomery, K. W. Kinzler, B. Vogelstein, A. Wissner, M. Nunes, P. Frost and C. M. Discafani, *Nat. Med.*, 2000, **6**, 1024.
20. J. Lehar, A. S. Krueger, W. Avery, A. M. Heilbut, L. M. Johansen, E. R. Price, R. J. Rickles, G. F. Short, 3rd, J. E. Staunton, X. Jin, M. S. Lee, G. R. Zimmermann and A. A. Borisy, *Nat. Biotechnol.*, 2009, **27**, 659.
21. L. Fan, F. Li, H. Zhang, Y. Wang, C. Cheng, X. Li, C. H. Gu, Q. Yang, H. Wu and S. Zhang, *Biomaterials*, 2010, **31**, 5634.
22. M. S. Muthu, S. A. Kulkarni, A. Raju and S. S. Feng, *Biomaterials*, 2012, **33**, 3494.
23. M. Khan, Z. Y. Ong, N. Wiradharma, A. B. Attia and Y. Y. Yang, *Adv. Healthc. Mater.*, 2012, **1**, 373.
24. S. Somasundaram, N. A. Edmund, D. T. Moore, G. W. Small, Y. Y. Shi and R. Z. Orlowski, *Cancer Res.*, 2002, **62**, 3868.
25. G. C. Jagetia and B. B. Aggarwal, *J. Clin. Immunol.*, 2007, **27**, 19.
26. J. W. Lown, *Pharmacol. Ther.*, 1993, **60**, 185.
27. J. Duan, H. M. Mansour, Y. Zhang, X. Deng, Y. Chen, J. Wang, Y. Pan and J. Zhao, *Int. J. Pharm.*, 2012, **426**, 193.
28. A. Goel and B. B. Aggarwal, *Nutr. Cancer*, 2010, **62**, 919.
29. C. Gong, B. Yang, Z. Qian, X. Zhao, Q. Wu, X. Qi, Y. Wang, G. Guo, B. Kan, F. Luo and Y. Wei, *Nanomed-Nanotechnol.*, 2012, **8**, 963.
30. R. R. Mehta, H. Katta, A. Kalra, R. Patel, A. Gupta, F. Alimirah, G. Murillo, X. Peng, A. Unni, M. Muzzio and R. G. Mehta, *Clin. Exp. Metastasis*, 2013, **30**, 855.
31. S. Xu, W. Wang, X. Li, J. Liu, A. Dong and L. Deng, *Eur. J. Pharm. Sci.*, 2014, **62**, 267.
32. A. Eldar-Boock, D. Polyak, A. Scomparin and R. Satchi-Fainaro, *Curr. Opin. Biotechnol.*, 2013, **24**, 682.
33. H. Wang, Y. Zhao, Y. Wu, Y. L. Hu, K. Nan, G. Nie and H. Chen, *Biomaterials*, 2011, **32**, 8281.
34. J. Y. Kim, G. Shim, H. W. Choi, J. Park, S. W. Chung, S. Kim, K. Kim, I. C. Kwon, C. W. Kim, S. Y. Kim, V. C. Yang, Y. K. Oh and Y. Byun, *Biomaterials*, 2012, **33**, 4424.
35. W. Dai, W. Jin, J. Zhang, X. Wang, J. Wang, X. Zhang, Y. Wan and Q. Zhang, *Pharm. Res.*, 2012, **29**, 2902.
36. R. Misra and S. K. Sahoo, *Mol. Pharm.*, 2011, **8**, 852.
37. D. Pramanik, N. R. Campbell, S. Das, S. Gupta, V. Chenna, S. Bisht, P. Sysa-Shah, D. Bedja, C. Karikari, C. Steenbergen, K. L. Gabrielson, A. Maitra and A. Maitra, *Oncotarget*, 2012, **3**, 640.
38. J. Fang, H. Nakamura and H. Maeda, *Adv. Drug. Deliv. Rev.*, 2011, **63**, 136.
39. M. A. Barry, C. A. Behnke and A. Eastman, *Biochem. Pharmacol.*, 1990, **40**, 2353.
40. Y. Sadzuka, M. Nagamine, T. Toyooka, Y. Ibuki and T. Sonobe, *Int. J. Pharm.*, 2012, **432**, 42.

Figure legends

Figure 1. Preparation and characterization of Dox-Cur-M. A: Schematic illustration of self-assembly of Dox-Cur-M; B: Particle size distribution of Dox-Cur-M; C: TEM image of Dox-Cur-M (Scale bar = 100 nm); D: Morphology of blank micelles (a), Dox- M (b), Cur-M (c), Dox-Cur-M (d).

Figure 2. *In vitro* release profile of Cur from Cur-M or Dox-Cur-M in PBS solution at pH 7.4 (A) or 10% FBS (C) and Dox from Dox-M or Dox-Cur-M in PBS solution at pH 7.4 (B) or 10% FBS (D), respectively. Error bars correspond to standard deviation.

Figure 3. Cytotoxicity studies of Dox-Cur-M. A: Cell viability of 4T1 cells after treatment with Cur-M, Dox-M and Dox-Cur-M does ranging from 0.039 to 2.5 μg/mL for 48 hours; B: Cell viability of 4T1 and L929 cells after exposure to different concentrations of mPEG-PCL copolymer. Error bars correspond to standard deviation.

Figure 4. Effects of Dox-Cur-M on the apoptosis of 4T1 breast tumor cells *in vitro*. Fluorescent microscopy of apoptotic cells induced by NS (A), blank micelles (B), Cur-M (C), Dox-M (D), Dox-Cur-M (E) and mean apoptotic index in each group (F). Scale bar = 100 μm. Error bars correspond to standard deviation.

Figure 5. Cellular uptake of doxorubicin in 4T1 cells. Fluorescence-activated cell sorting analysis of 4T1 cells after exposure to blank micelles (control), free Dox, Dox-M, free (Dox + Cur), Dox-M + free Cur and Dox-Cur-M at a final doxorubicin concentration of 500 ng/mL of 2h (A) and 4h (B); The percentage of doxorubicin-containing cells in each group at 2h (C) and 4h (D); The mean of

fluorescence intensity in each group at 2h (E) and 4h (F). Error bars correspond to standard deviation.

Figure 6. Images of cellular uptake assays. Fluorescent images of cells exposed to blank micelles, Dox-M and Dox-Cur-M for 2h and 4h under a fluorescence microscope, showing nuclear staining using Hoechst33258 (blue) and doxorubicin-derived fluorescence (red) in the nuclei. Scale bar = 100 μm.

Figure 7. Antitumor effect of NS (control), blank micelles, Cur-M, Dox-M, and Dox-Cur-M in subcutaneous 4T1 model, respectively. A: Photographs of a tumor from each treatment excised on day 30 (scale bar = 1 cm); B: Tumor growth curve of each group; C: Weight of subcutaneous tumors in each group. Error bars correspond to standard deviation.

Figure 8. Pulmonary metastasis in subcutaneous 4T1 model. A: Representative photographs of pulmonary metastatic tumors in each group (scale bar = 2 cm); B: Number of tumor nodules in each group; C: Weight of lungs in each group. Error bars correspond to standard deviation.

Figure 9. TUNEL staining of tumors in each group. Representative TUNEL staining images of NS (A), blank micelles (B), Cur-M (C), Dox-M (D) and Dox-Cur-M (E) and mean Apoptotic index in each group (F). Scale bar = 100 μm. Error bars correspond to standard deviation.

Figure 10. Ki-67 immunohistochemical staining of tumors. Representative Ki-67 immunohistochemical images of NS (A), blank micelles (B), Cur-M (C), Dox-M (D)

and Dox-Cur-M (E) and mean Ki-67 LI in each group (F). Scale bar = 100 μm.Error bars correspond to standard deviation.

Figure 11. CD31 immunofluorescent staining of tumors. Representative CD31 immunofluorescent images of NS (A), blank micelles (B), Cur-M (C), Dox-M (D) and Dox-Cur-M (E) and MVD in each group (F). Scale bar = 100 μm. Error bars correspond to standard deviation.

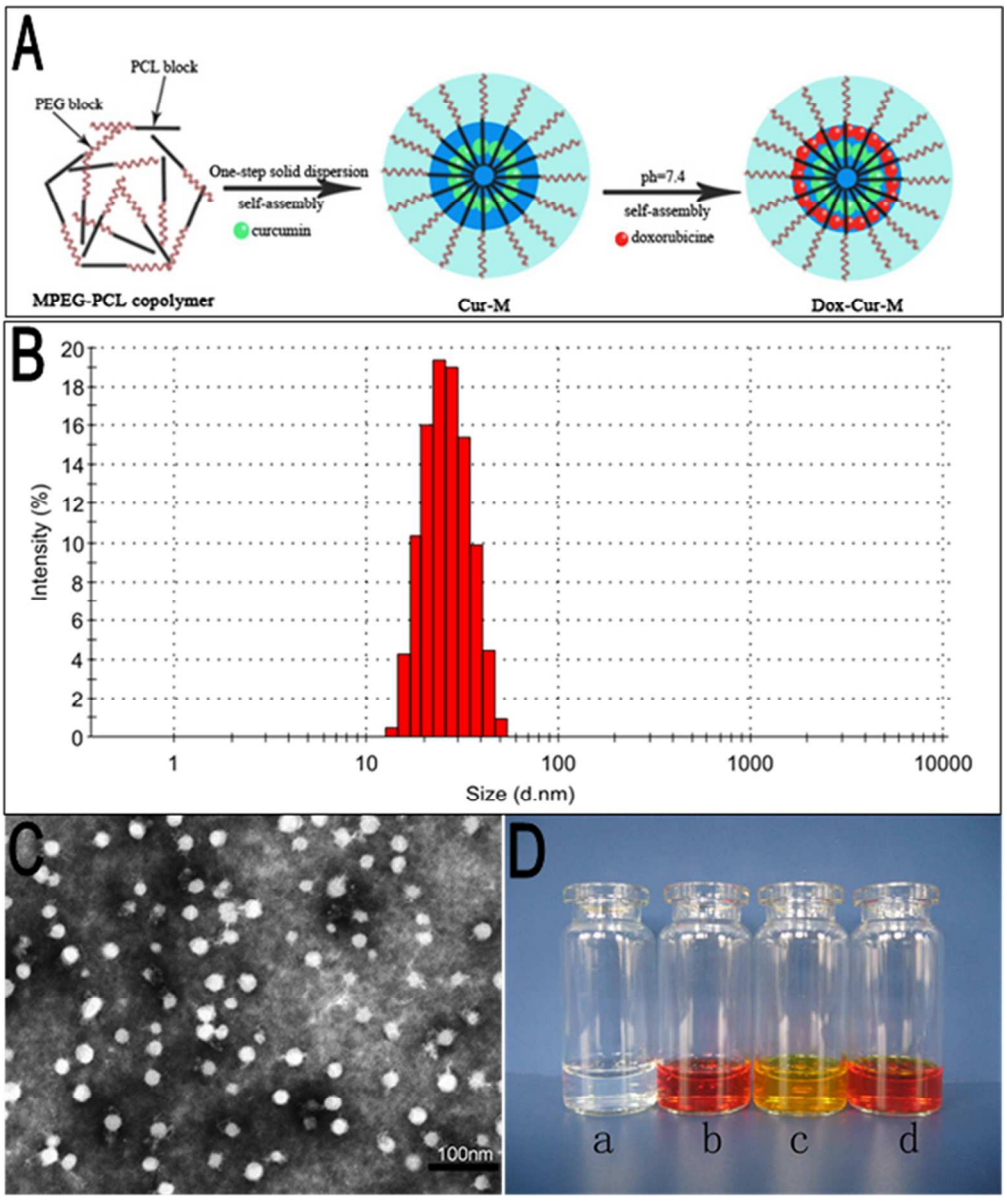

Preparation and characterization of Dox-Cur-M. A: Schematic illustration of self-assembly of Dox-Cur-M; B: Particle size distribution of Dox-Cur-M; C: TEM image of Dox-Cur-M (Scale bar = 100 nm); D: Morphology of blank micelles (a), Dox- M (b), Cur-M (c), Dox-Cur-M (d).
127x151mm (300 x 300 DPI)

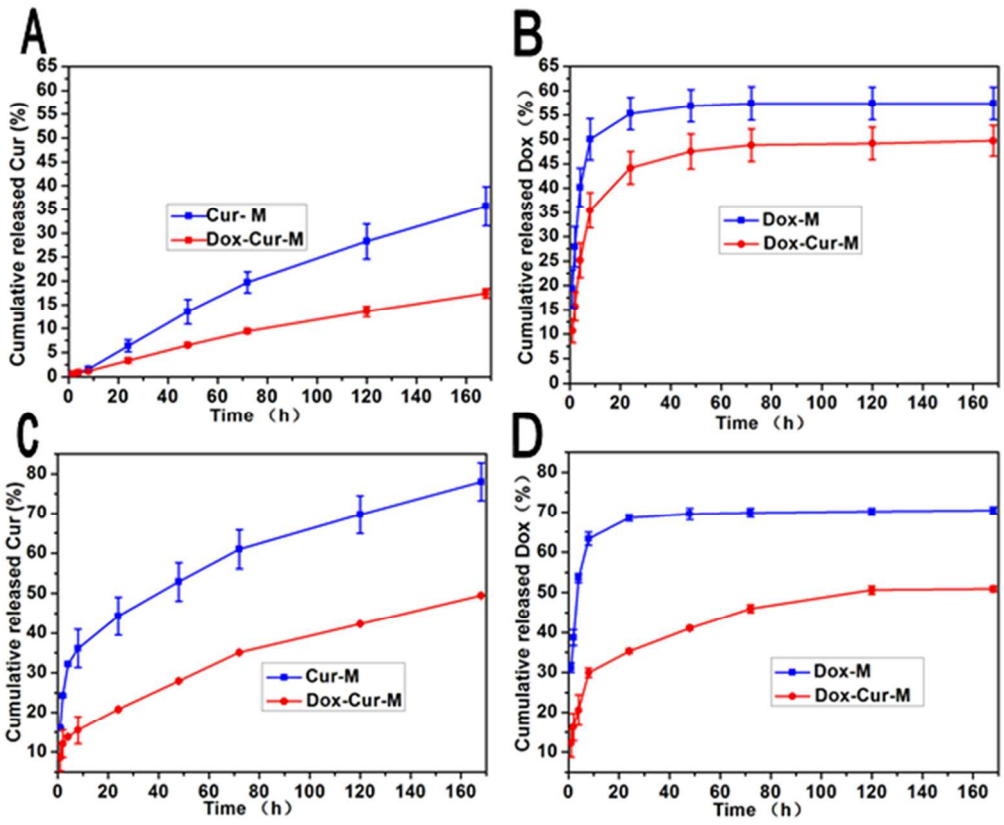

In vitro release profile of Cur from Cur-M or Dox-Cur-M in PBS solution at pH 7.4 (A) or 10% FBS (C) and Dox from Dox-M or Dox-Cur-M in PBS solution at pH 7.4 (B) or 10% FBS (D), respectively. Error bars correspond to standard deviation.
127x103mm (300 x 300 DPI)

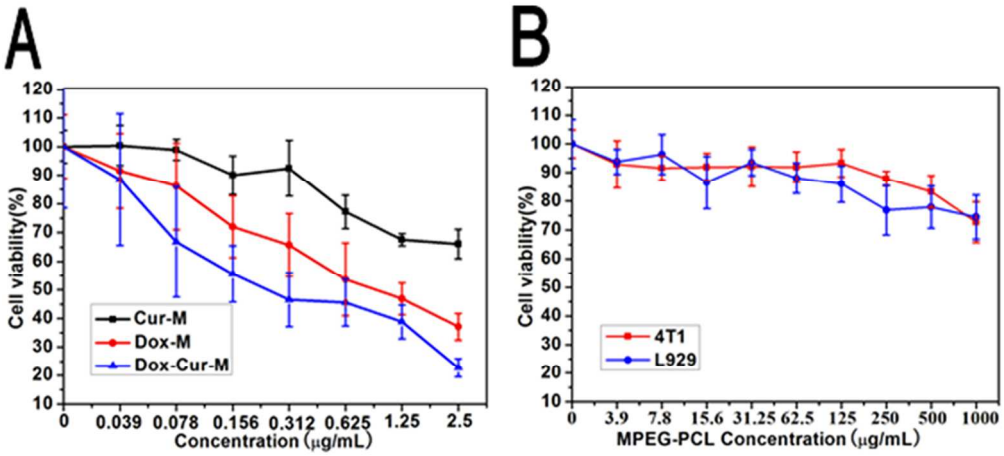

Cytotoxicity studies of Dox-Cur-M. A: Cell viability of 4T1 cells after treatment with Cur-M, Dox-M and Dox-Cur-M does ranging from 0.039 to 2.5 μg/mL for 48 hours; B: Cell viability of 4T1 and L929 cells after exposure to different concentrations of mPEG-PCL copolymer. Error bars correspond to standard deviation.
127x58mm (300 x 300 DPI)

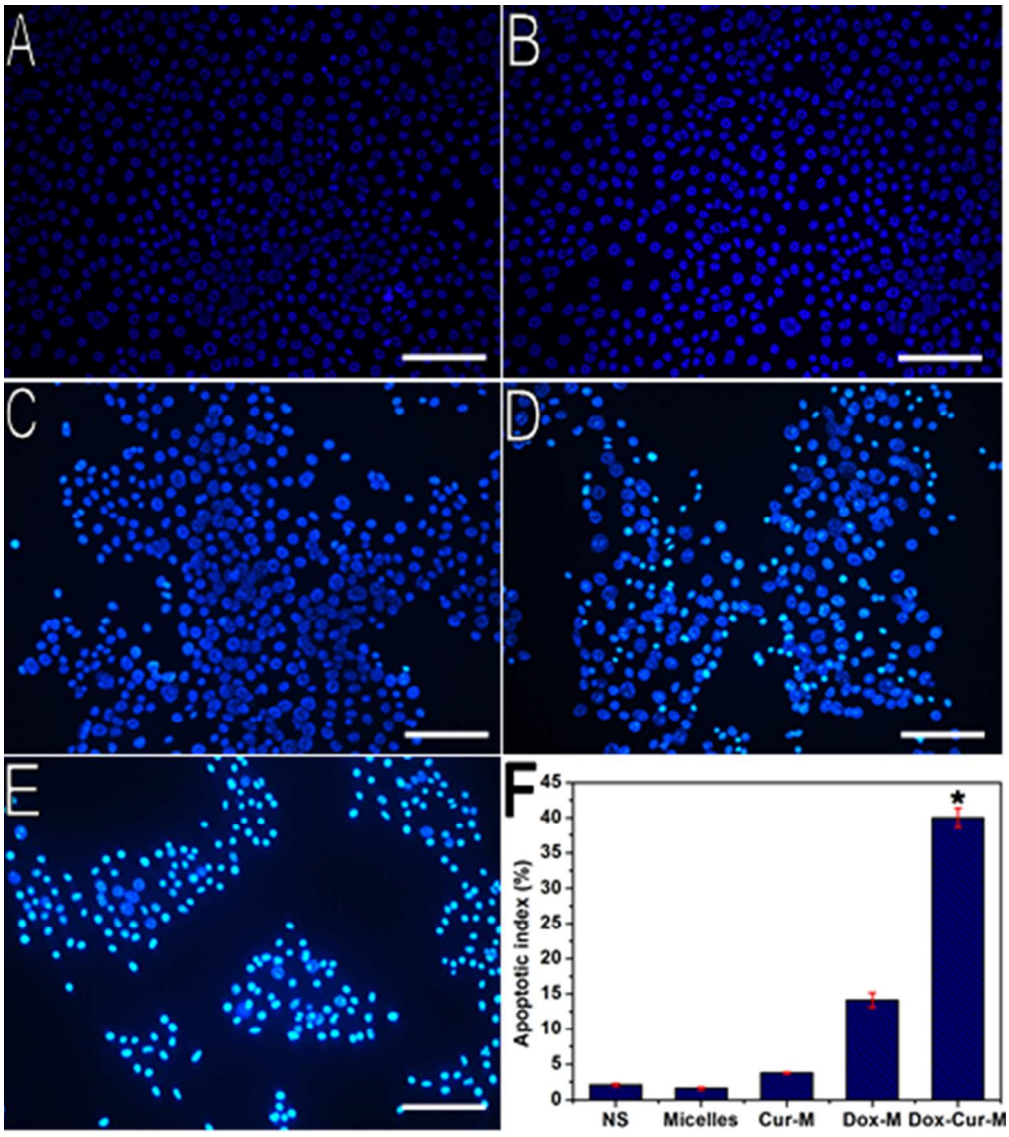

Effects of Dox-Cur-M on the apoptosis of 4T1 breast tumor cells in vitro. Fluorescent microscopy of apoptotic cells induced by NS (A), blank micelles (B), Cur-M (C), Dox-M (D), Dox-Cur-M (E) and mean apoptotic index in each group (F). Scale bar = 100 μm. Error bars correspond to standard deviation.
127x143mm (300 x 300 DPI)

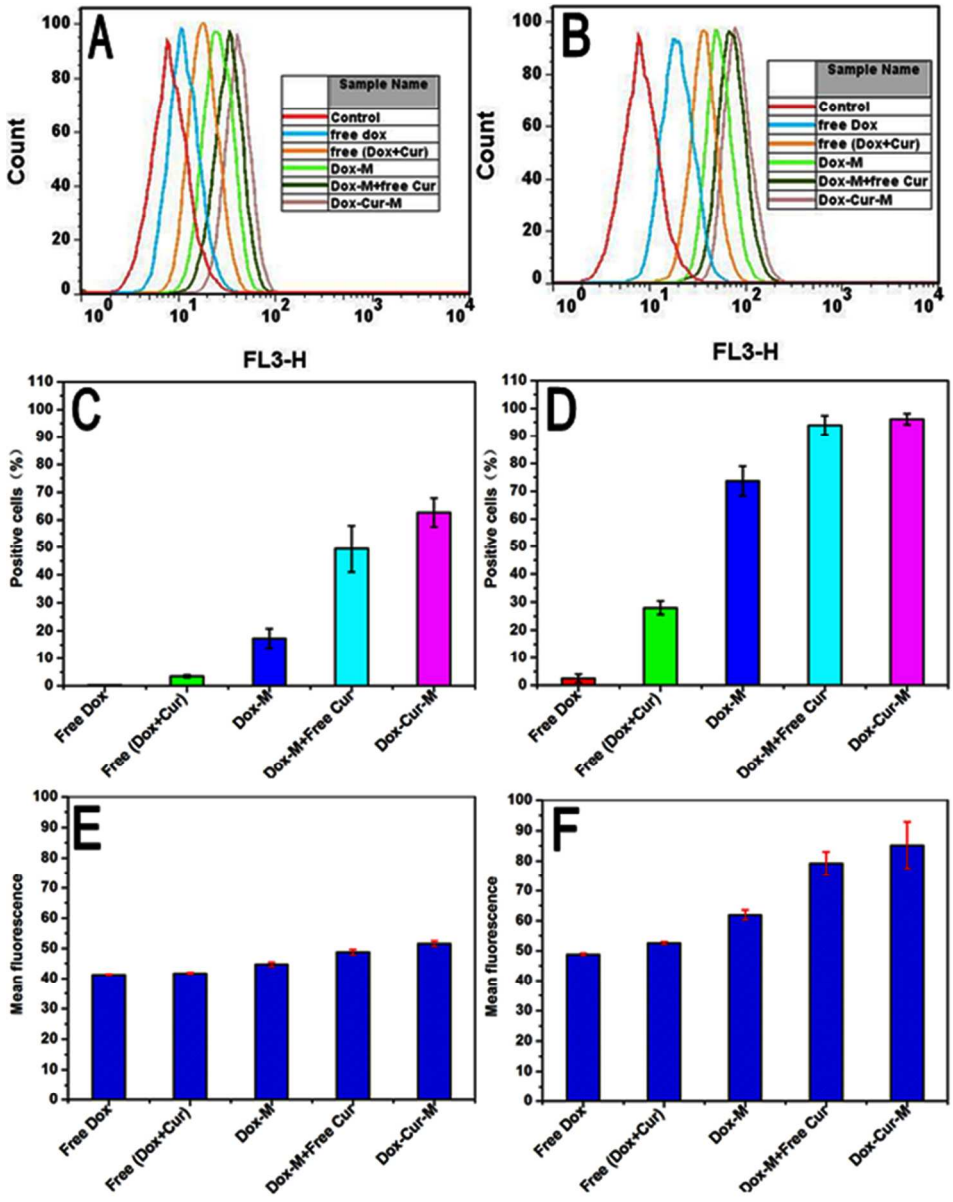

127x161mm (300 x 300 DPI)

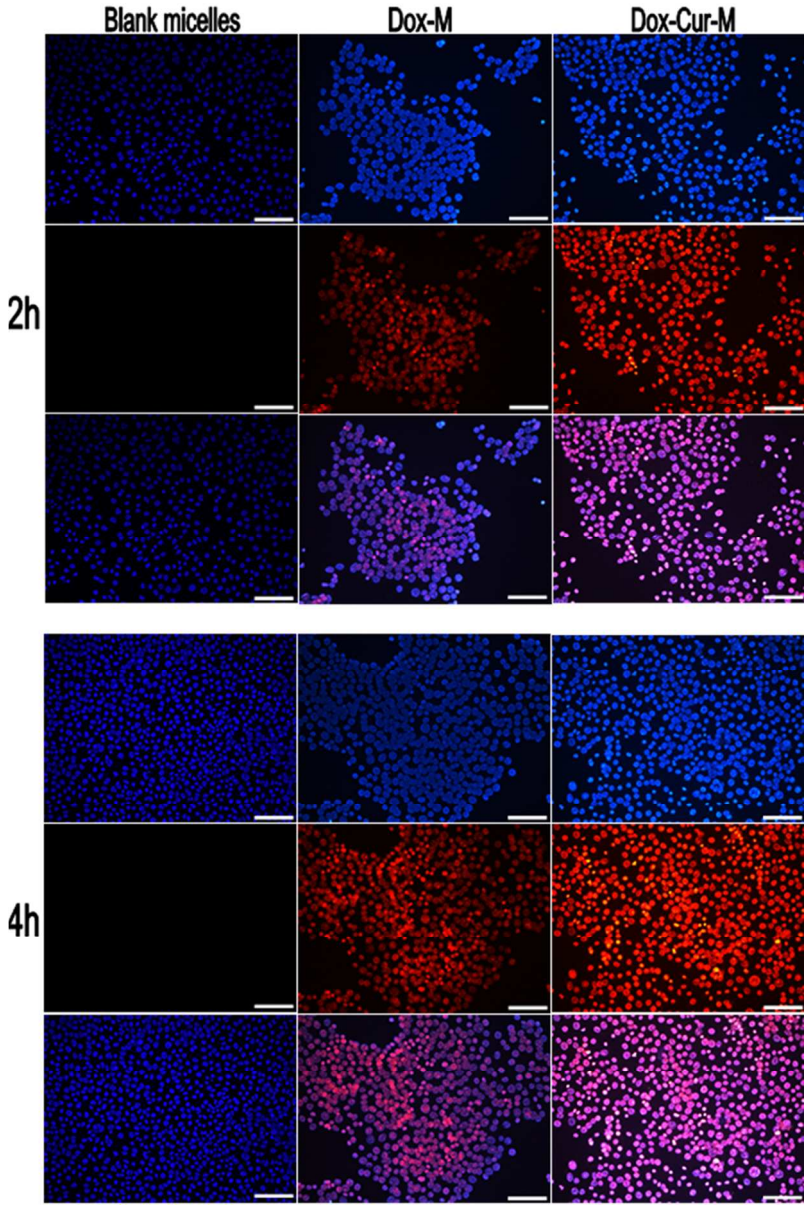

Images of cellular uptake assays. Fluorescent images of cells exposed to blank micelles, Dox-M and Dox-Cur-M for 2h and 4h under a fluorescence microscope, showing nuclear staining using Hoechst33258 (blue) and doxorubicin-derived fluorescence (red) in the nuclei. Scale bar = 100 μm.
127x191mm (300 x 300 DPI)

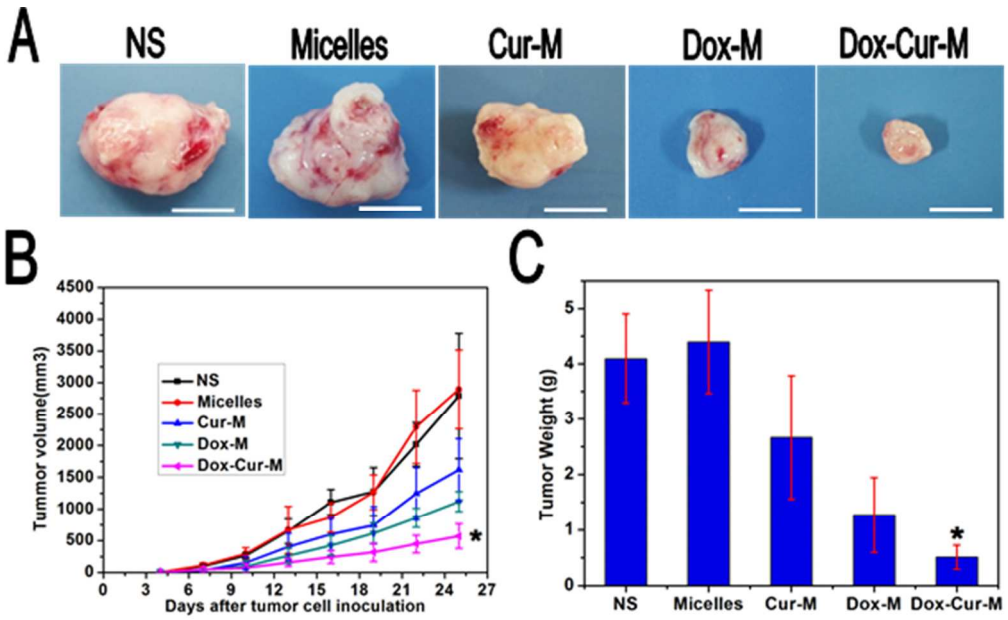

Antitumor effect of NS (control), blank micelles, Cur-M, Dox-M, and Dox-Cur-M in subcutaneous 4T1 model, respectively. A: Photographs of a tumor from each treatment excised on day 30 (scale bar = 1 cm); B: Tumor growth curve of each group; C: Weight of subcutaneous tumors in each group. Error bars correspond to standard deviation.
128x78mm (300 x 300 DPI)

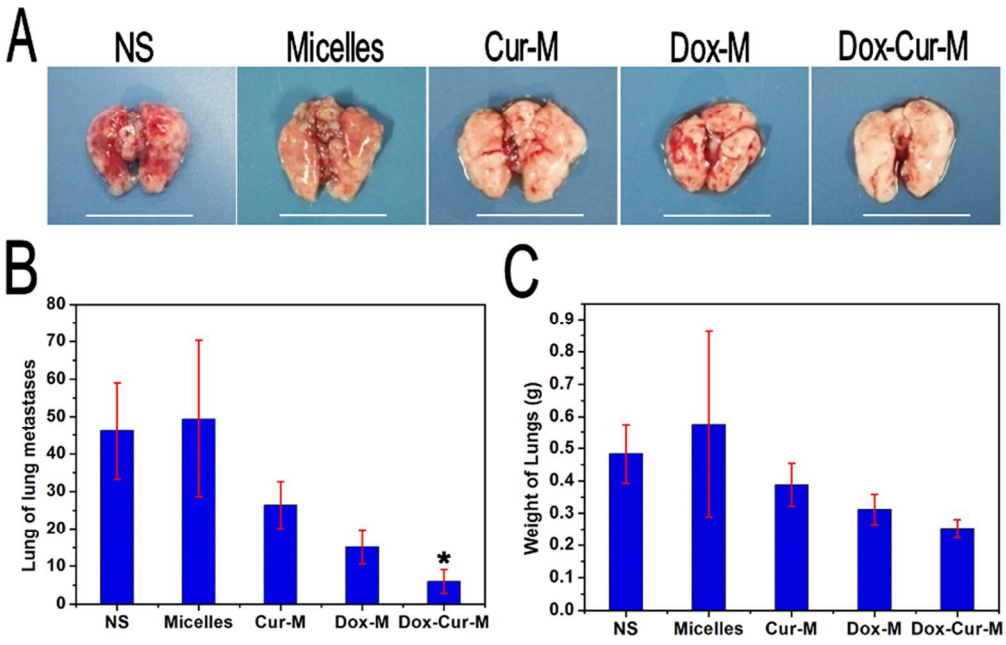

Pulmonary metastasis in subcutaneous 4T1 model. A: Representative photographs of pulmonary metastatic tumors in each group (scale bar = 2 cm); B: Number of tumor nodules in each group; C: Weight of lungs in each group. Error bars correspond to standard deviation.
127x79mm (300 x 300 DPI)

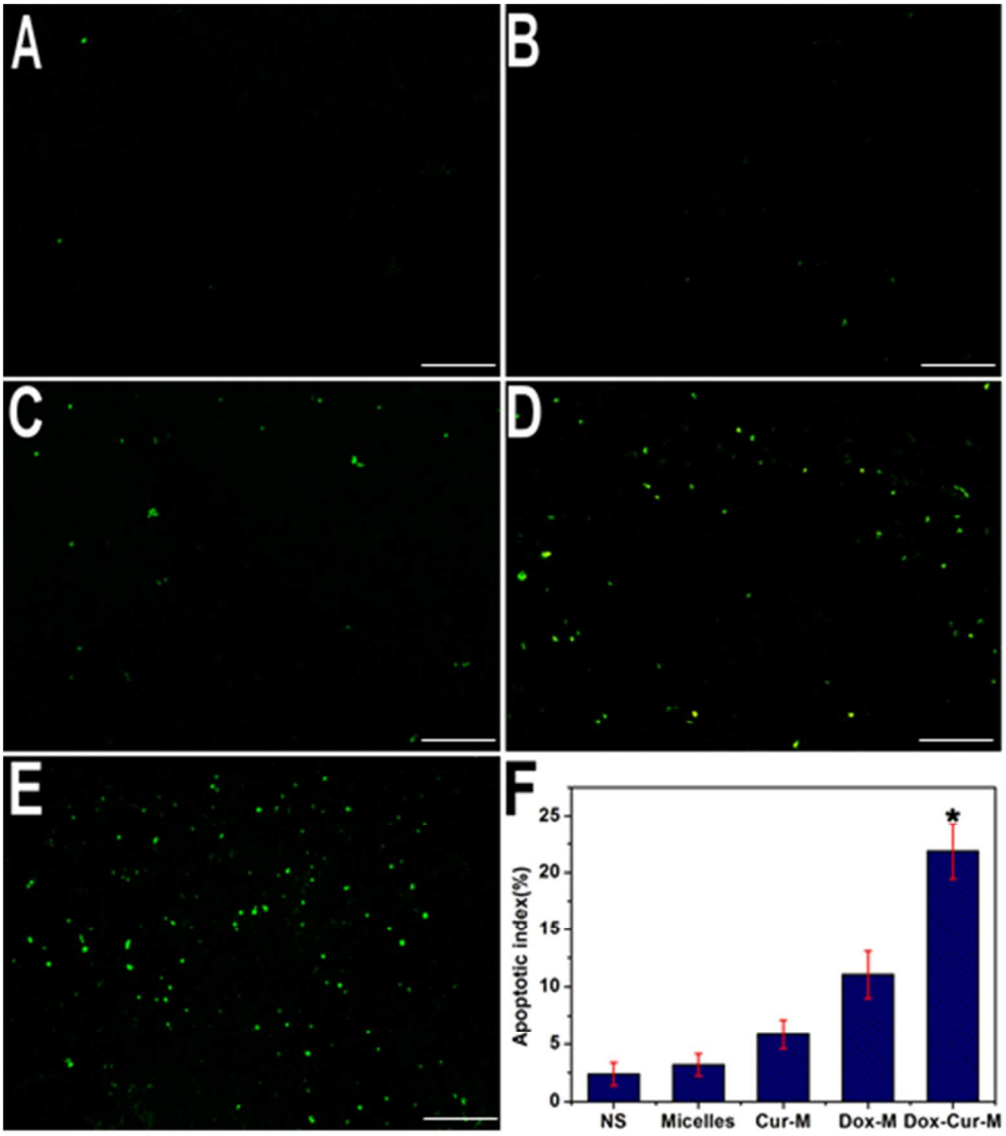

TUNEL staining of tumors in each group. Representative TUNEL staining images of NS (A), blank micelles (B), Cur-M (C), Dox-M (D) and Dox-Cur-M (E) and mean Apoptotic index in each group (F). Error bars correspond to standard deviation.
127x143mm (300 x 300 DPI)

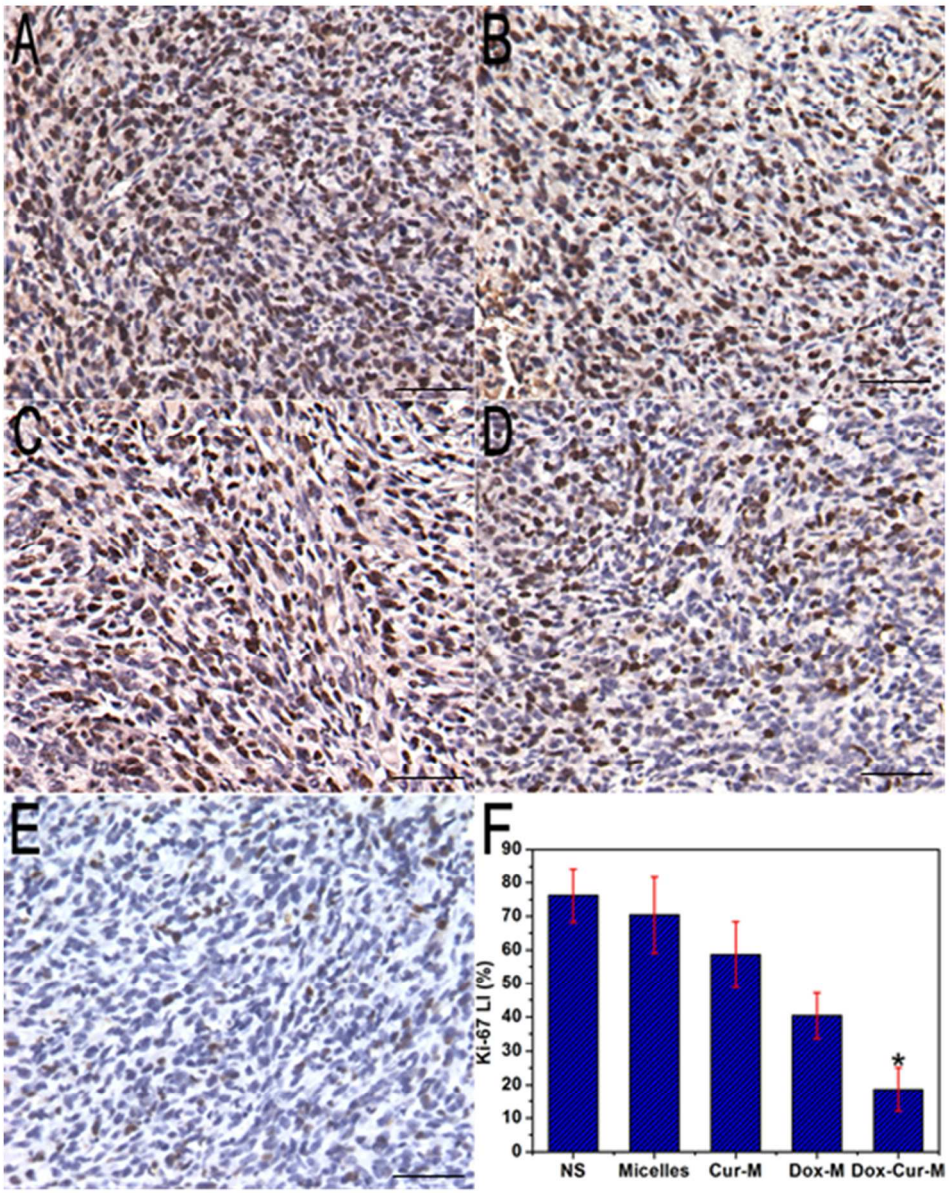

Ki-67 immunohistochemical staining of tumors. Representative Ki-67 immunohistochemical images of NS (A), blank micelles (B), Cur-M (C), Dox-M (D) and Dox-Cur-M (E) and mean Ki-67 LI in each group (F). Error bars correspond to standard deviation.
127x161mm (300 x 300 DPI)

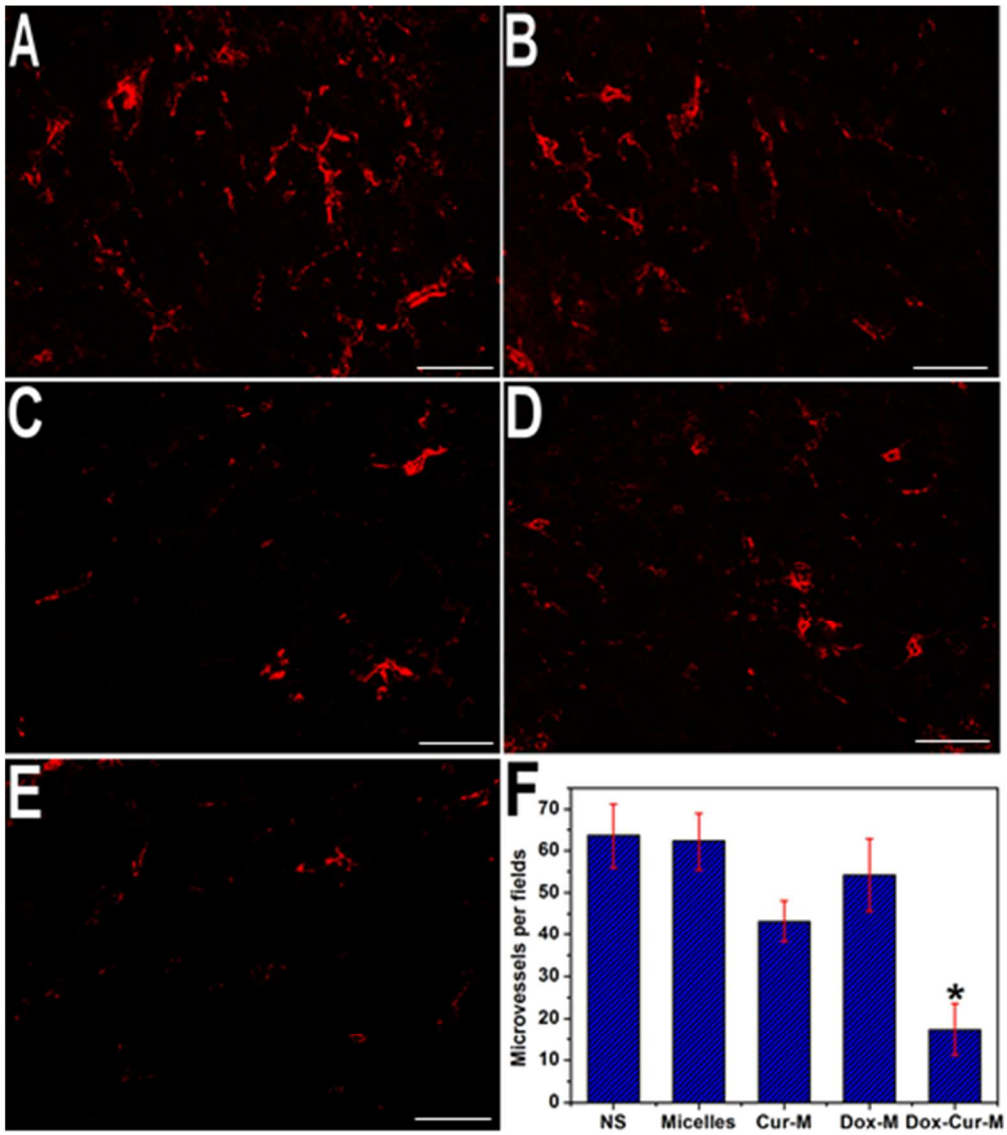

CD31 immunofluorescent staining of tumors. Representative CD31 immunofluorescent images of NS (A), blank micelles (B), Cur-M (C), Dox-M (D) and Dox-Cur-M (E) and MVD in each group (F). Error bars correspond to standard deviation.
127x143mm (300 x 300 DPI)

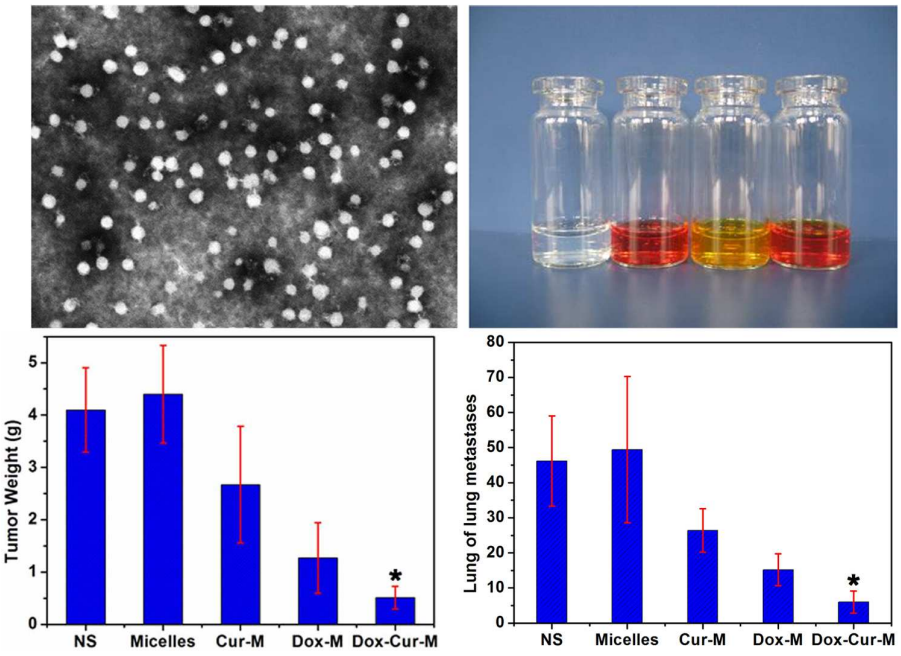

In this work, we used polymeric micelles to co-delivery hydrophilic doxorubicin and hydrophobic curcumin simultaneously to achieve combination therapy. The prepared doxorubicin-curcumin micelles improved cytotoxicity, apoptosis, and cellular uptake *in vitro* and enhanced antitumor and anti-metastasis activity *in vivo* on breast carcinoma.